OSBPL3-Driven Sterol Metabolic Reprogramming Promotes Oncogenic Signaling and Therapeutic Resistance in Pancreatic Cancer

Running title: OSBPL3 in PDA Progression

Qihui Sun[1,3#], Xiaojia Li[1,3#], Qi Zou[1,2,3#], Yang Chen[1,3], Xiaoqi Zhu[1,2,3], Hailin Jiang[1,3], Tingting Jiang[1,3], Fang Wei[1,2,3], Keping Xie[1,2,3*]

[1]Center for Pancreatic Cancer Research, The South China University of Technology School of Medicine, Guangzhou, Guangdong 510006, China

[2]Guangzhou Digestive Disease Center, Guangzhou First People's Hospital and The Second Affiliated Hospital, South China University of Technology School of Medicine, Guangzhou, China

[3]The South China University of Technology Comprehensive Cancer Center, Guangzhou, Guangdong 510006, China

[*]*Correspondence authors*: Keping Xie or Fang Wei, Center for Pancreatic Cancer Research, South China University of Technology School of Medicine, Guangzhou 510006, China; *E-mail*: mcxiekeping@scut.edu.cn.

Disclosure of Potential Conflicts of Interest: The authors declare no conflict of interest.

[#]Q. Sun，X. Li and Q. Zou have contributed equally to this work and are considered co-first authors.

Supplementary Figures

A GSE155698

Granulocytes
T Cells
Ductal cells
Macrophages
Acinar cells
Erythrocytes
DC
Fibroblasts

Plasma cells
Pericytes
EC
Monocytes
B cells
Mast cells
Metaplastic cells

OSBPL3

B GSE226829

P = 4.7e-07

C Expression level of OSBPL3

P = 3.4e-50

Normal (n = 74)
Tumor (n = 137)

D

GSE16515	GSE32672	GSE62452	GSE71729
P = 2.4e-05	P = 0.026	P = 1e-13	P < 2.2e-16

Normal Tumor

E TCGA

event
death
alive

riskgroup
high
low

F TCGA

Points

OSBPL3

residual

age

stage

response

Total Points

Linear Predictor

1−year Survival Probability

3−year Survival Probability
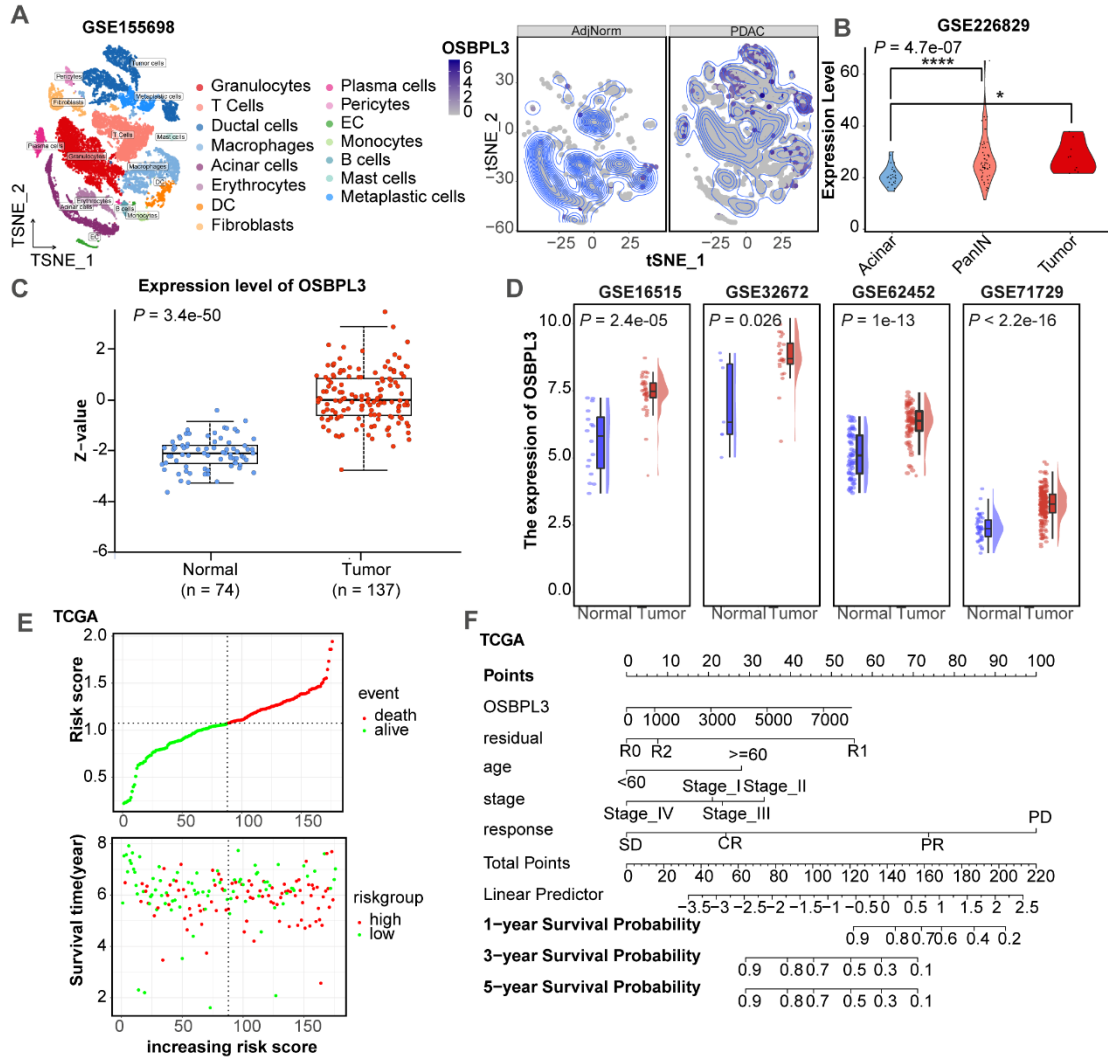
5−year Survival Probability

Figure S1. High expression of OSBPL3 in pancreatic cancer and precancerous lesions correlates with poor prognosis in human PDA Samples

(**A**) UMAP plot showing the clustering of 15 cell groups derived from single-cell transcriptomic data of 16 PDA tissues and 3 adjacent normal tissues from the GSE155698 dataset. The expression density map reveals significantly higher OSBPL3 expression in tumor tissues, predominantly within tumor cells.

(**B**) OSBPL3 expression across acinar cells, PanIN lesions, and tumor cell regions in the GSE226829 dataset. Cells from different regions are represented in distinct colors.

(**C**) Boxplot showing the protein expression of OSBPL3 in PDA and adjacent normal tissues from the CPTAC dataset in the UALCAN database (n = 211).

(**D**) OSBPL3 expression levels in PDA tissues compared to normal control tissues across transcriptomic datasets (GSE16515, GSE32672, GSE62452, GSE71729) from the GEO database. Blue: normal control group; Red: tumor tissue group.

(**E**) Risk factor density map showing OSBPL3 expression in PDA.

(**F**) Nomogram illustrating 1-, 3- and 5-year survival predictions based on OSBPL3 expression levels, age, stage and other prognostic factors.
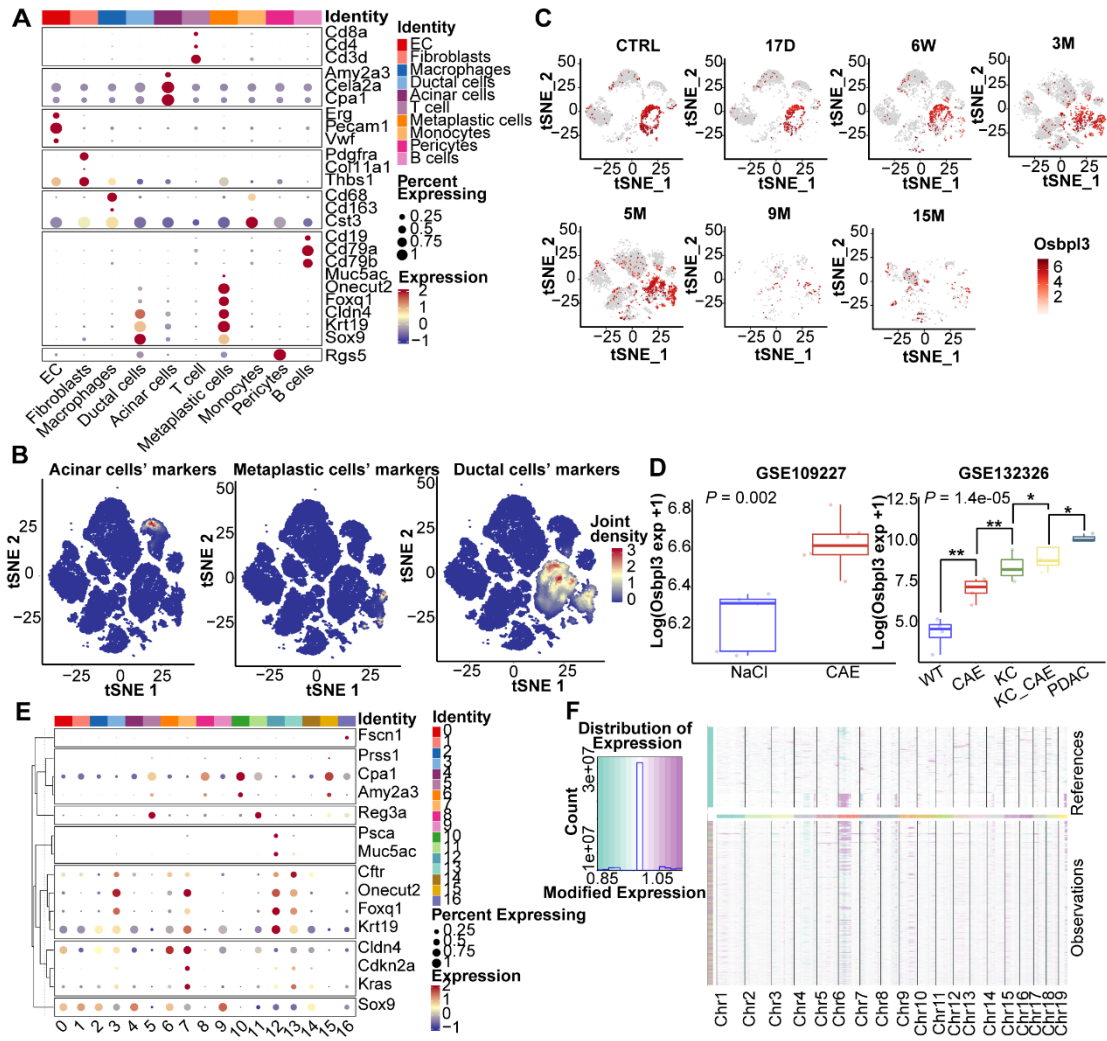
Figure S2. Expression of Osbpl3 increases progressively during PDA initiation and progression.

(**A**) Dot plot showing the percentage of expressed cells and the average expression levels of canonical marker genes for major cell types across 10 distinct cell clusters (cohort: GSE141017).

(**B**) Density distribution of signature gene sets for acinar cells (Cpa1, Cela2a, and Amy2a), ductal cells (Krt19, Sox9, and Cldn4), and metaplastic cells (Onecut2, Foxq1, and Muc5ac) across different cell subpopulations

(**C**) Single-cell expression of Osbpl3 across different cell subpopulations at various time points from the GSE141017 dataset, which models PDA progression in the KC mouse model.

(**D**) OSBPL3 expression levels in normal, pancreatitis, and PDA samples from the GSE109227 and GSE132326 datasets.

(**E**) Bubble plot depicting the expression of marker genes for acinar, ductal, and malignant cells across different epithelial subpopulations.

(**F**) Copy number prediction of epithelial cells at various time points, with the CTRL group as a reference, based on the inferCNV algorithm.
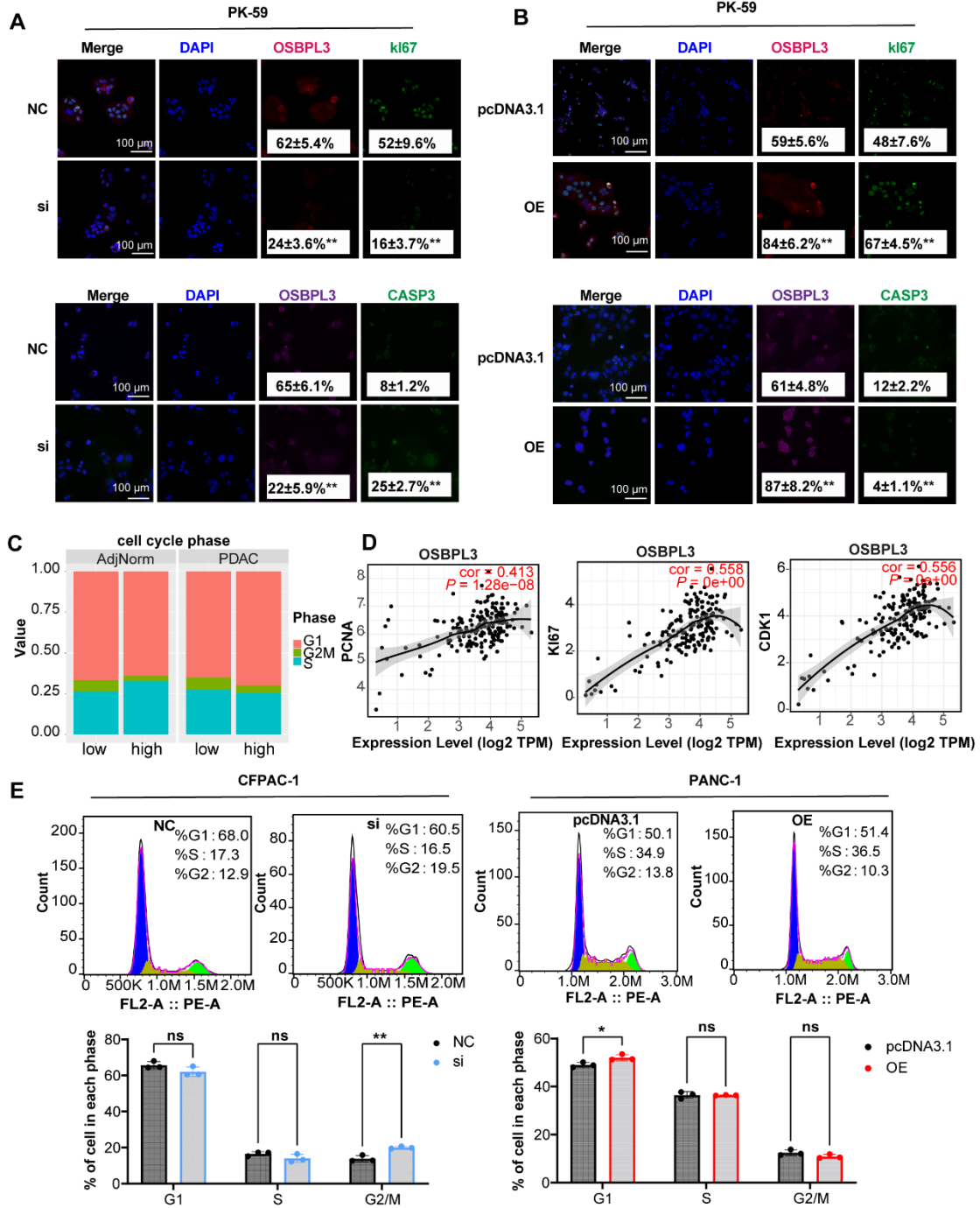
Figure S3. Role of OSBPL3 in PDA cell proliferation.

(**A**) and (**B**) Immunofluorescence staining in the PK-59 PDA cell line to assess the expression of proliferation (Ki67) and apoptosis (CASP3) markers before and after OSBPL3 knockdown or overexpression. Magnification: 20x. DAPI (blue) marks cell nuclei, red and purple fluorescence indicate OSBPL3 expression (mainly in the cytoplasm), and green fluorescence represents Ki67 (nuclear) and CASP3 (cytoplasmic) expression.

(**C**) Proportion of cells in different cell cycle phases in the human PDA and adjacent tissue single-cell dataset GSE155698. The stacked bar chart shows the percentage of cells at each cell cycle phase, grouped by high and low OSBPL3 expression levels, and further stratified by tumor or adjacent tissue origin.

(**D**) Correlation analysis between OSBPL3 expression and the proliferation-related genes PCNA, MKI67 and CDK1.

(**E**) Flow cytometry analysis of cell cycle changes following OSBPL3 knockdown or overexpression. The bar chart shows the differences in the proportions of cells at various cell cycle phases between the two groups.
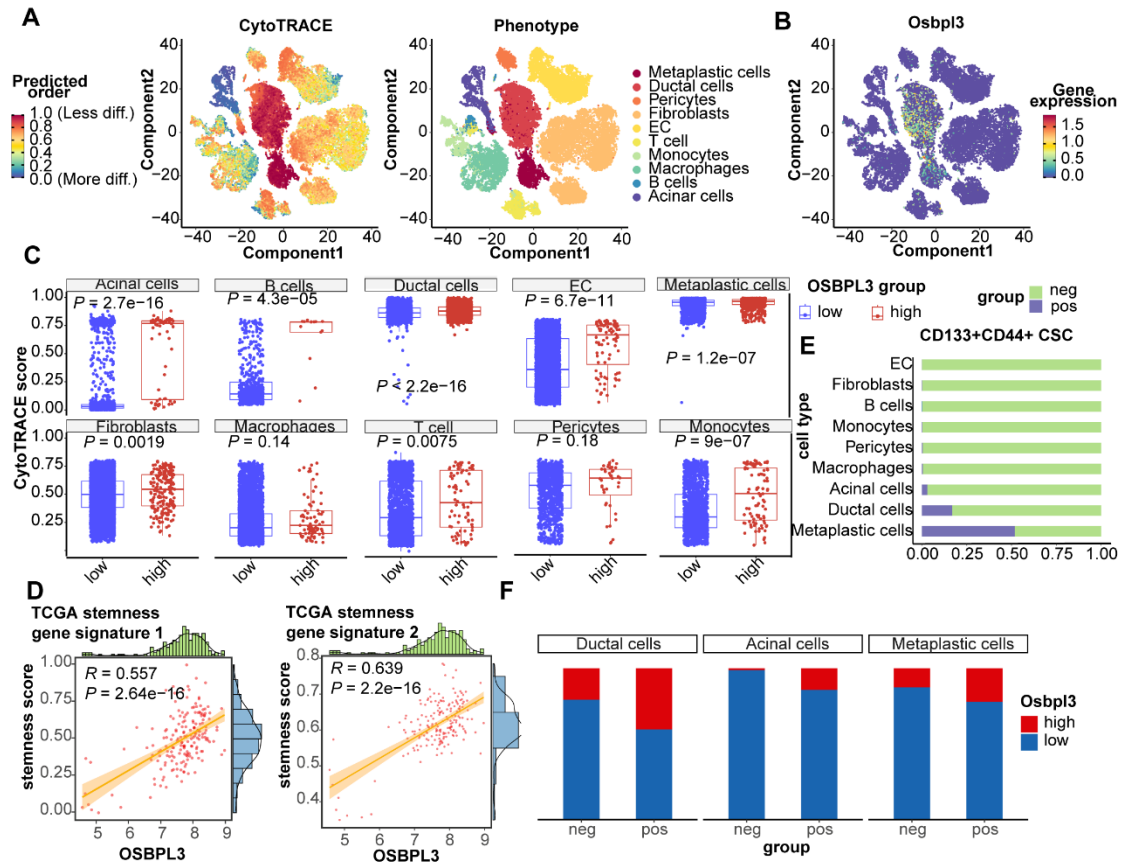
Figure S4. The role of OSBPL3 in tumor stemness in PDA.

(**A**) Dimensionality reduction plot based on CytoTRACE pseudotime analysis showing stemness prediction scores for single-cell samples from the KC pancreatic mouse model.

(**B**) The plot represents CytoTRACE predicted scores, along with OSBPL3 gene expression.

(**C**) Faceted boxplot showing the CytoTRACE predicted stemness scores for cells with high or low OSBPL3 expression across different cell subpopulations.

(**D**) Correlation between the GSVA scores of two tumor stemness gene sets and OSBPL3 expression in TCGA-PAAD pancreatic cancer transcriptomic data.

(**E**) and (**F**) Bar chart displaying the proportion of tumor stem cells based on CD133 and CD44 marker gene annotations in various cell subpopulations, as well as the proportion of tumor stem cells in acinar cells, ductal cells, and metaplastic cells, comparing OSBPL3 high and low expression groups.
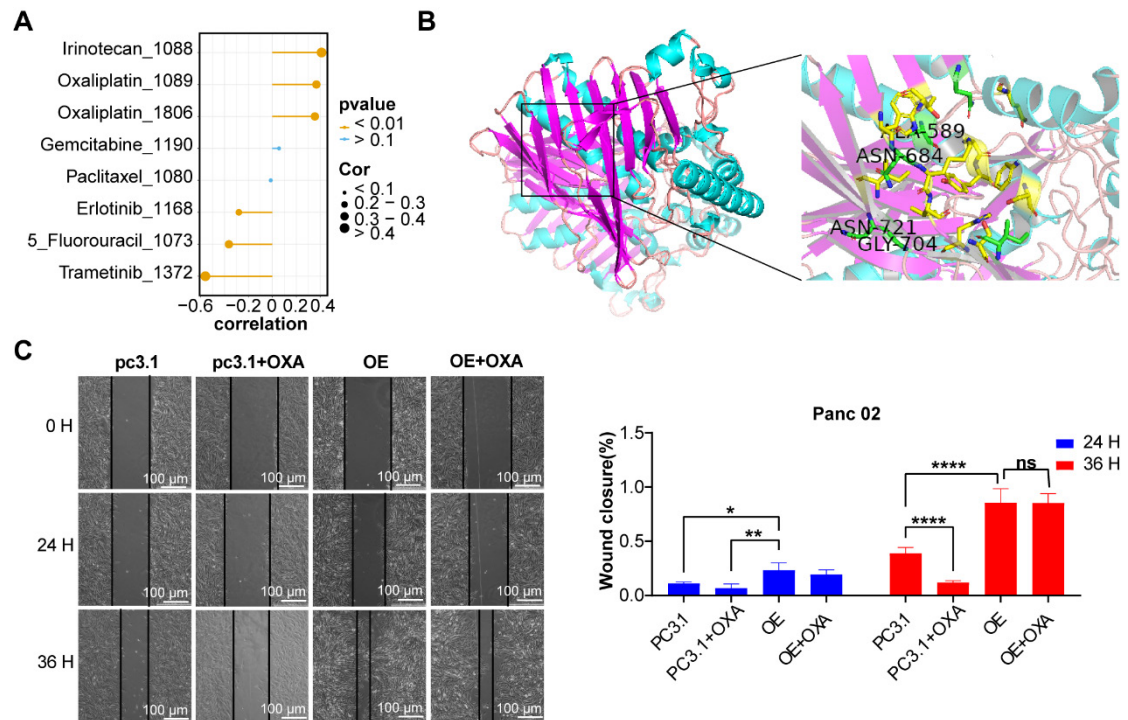
Figure S5. High expression of OSBPL3 reverses the inhibitory effect of oxaliplatin on PDA cell migration.

(**A**) Lollipop plot showing the correlation between OSBPL3 expression and the IC50 values of common pancreatic cancer chemotherapy drugs. Orange represents *P*-value < 0.05, while blue represents *P*-value > 0.1. The length of the line and the size of the circle are positively correlated with the correlation value.

(**B**) Molecular docking prediction of the binding sites between OSBPL3 and oxaliplatin.

(**C**) Representative images from the wound healing assay to assess cell migration in the Panc02 PDA cell line, following changes in Osbpl3 expression and oxaliplatin treatment. The bar chart shows statistical analysis of cell migration rates at 12 and 24 h time points. Blue and red represent migration rates at 12 and 24 h, respectively. ANOVA and multiple t-tests were performed. ns indicates no significant difference, *P < 0.05, **P < 0.01, ***P < 0.001, ****P < 0.0001.
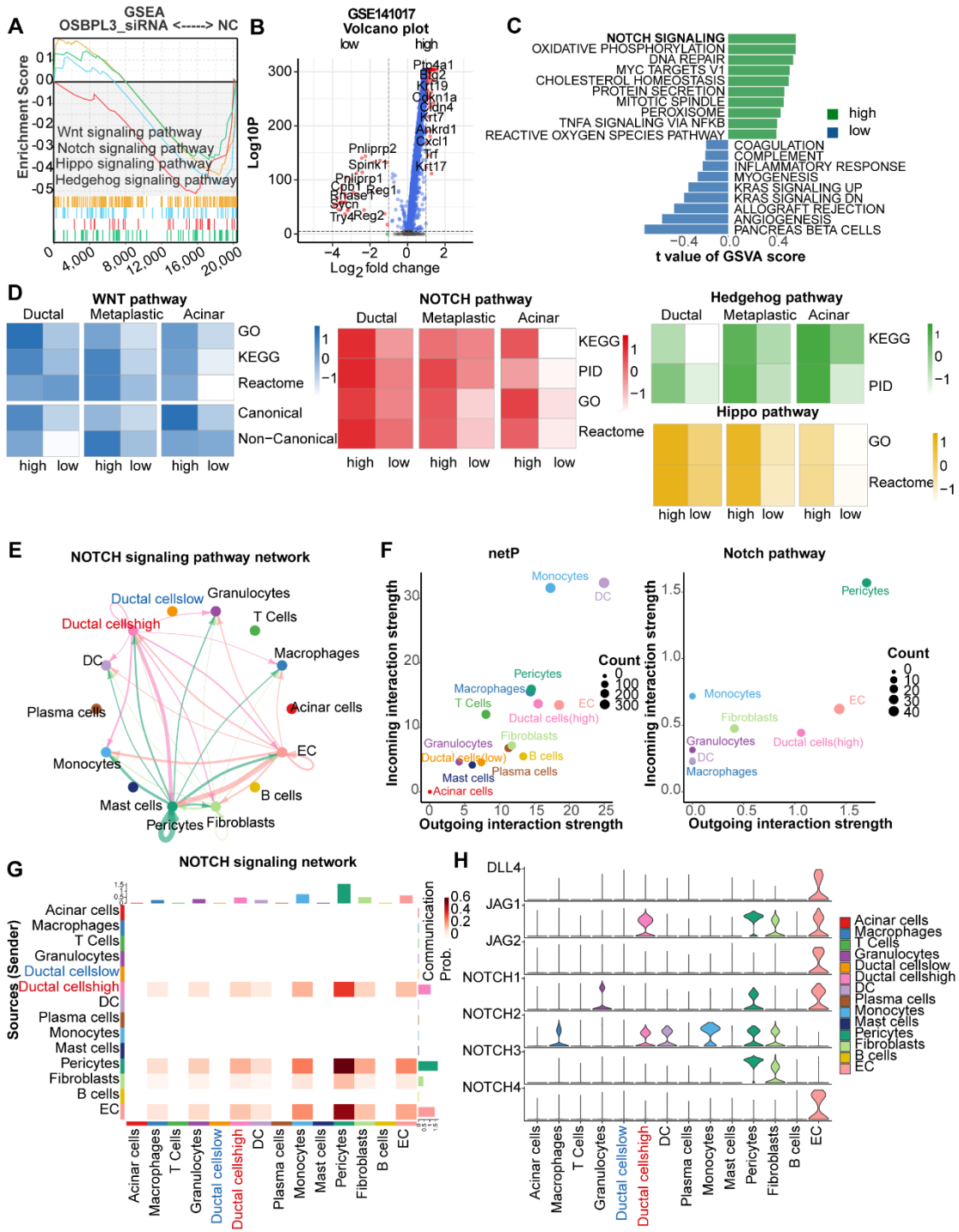
Figure S6. OSBPL3 overexpression group shows significant activation of pathways such as NOTCH

(**A**) GSEA analysis of stemness-related regulatory pathways in CFPAC-1 cells, comparing to NC and OSBPL3 Si groups.

(**B**) Volcano plot illustrating differentially expressed genes between the high and low OSBPL3 expression groups in epithelial cell subpopulations extracted from the KC mouse single-cell dataset (GSE141017).

(**C**) Waterfall plot presenting the enrichment analysis of HALLMARK pathways for the high and low OSBPL3 expression groups.

(**D**) GSVA scores for stemness-regulating pathways such as NOTCH and WNT in different cell subpopulations based on high or low OSBPL3 expression.

(**E**) Cell-cell communication network analysis of NOTCH pathway-related interactions between different cell types in PDA tissues.

(**F**) Cell communication intensity for different cell types, along with the communication strength related to the NOTCH pathway.

(**G**) Heatmap displaying NOTCH pathway-related communication networks when different cell types act as signal senders or receivers.

(**H**) Violin plot illustrating the distribution of gene expression for NOTCH signaling-related genes across different cell types.
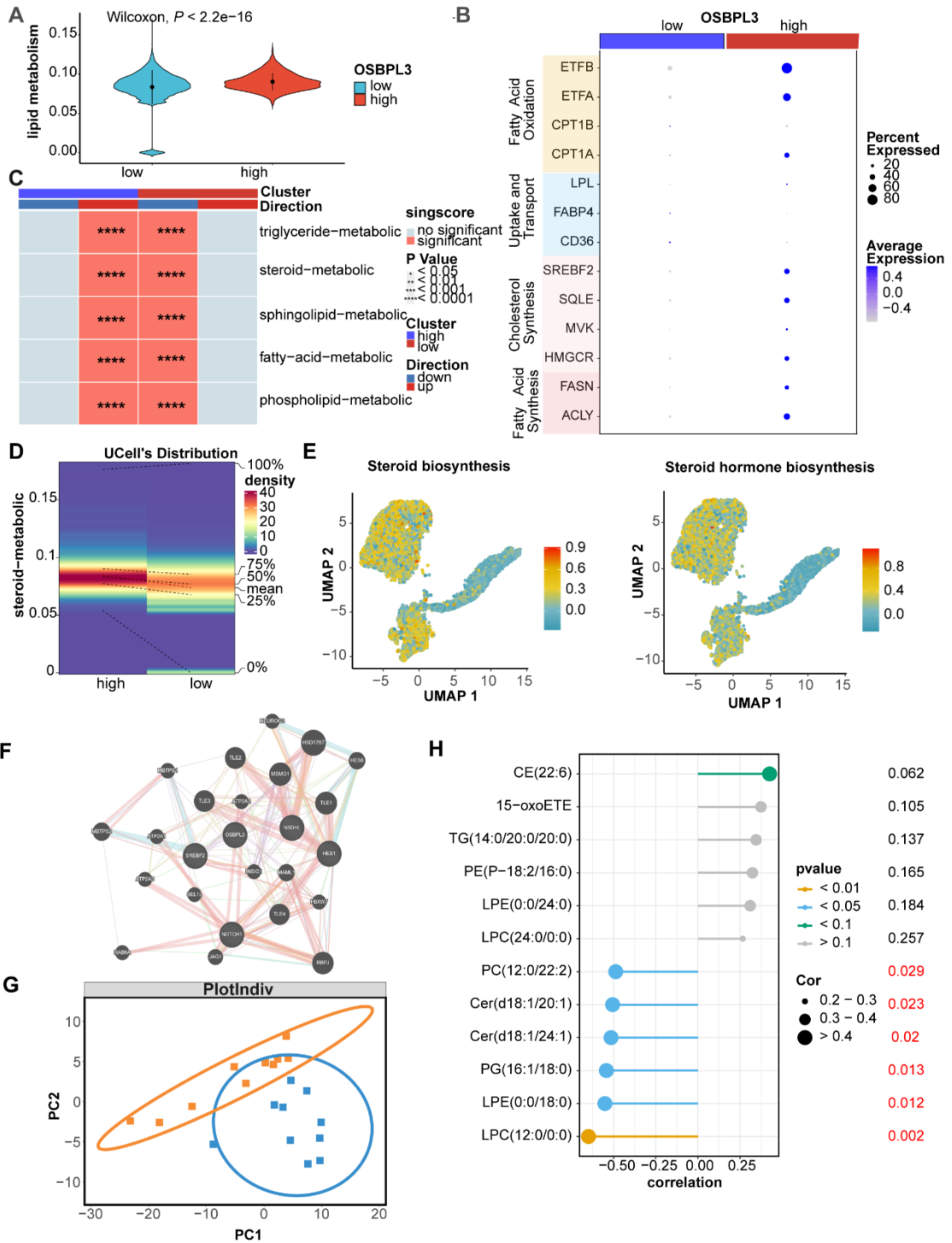
Figure S7. OSBPL3 Overexpression Contributes to Increased Cholesterol synthesis in PDA

(**A**) Violin plot showing lipid metabolism scores between OSBPL3 high and low expression groups in the single-cell dataset GSE155698. Lipid metabolism scores were calculated using the AddModuleScore algorithm. Statistical significance was assessed using the two-sided Wilcoxon rank-sum test. *$P < 0.05$, **$P < 0.01$, ***$P < 0.001$, ****$P < 0.0001$.

(**B**) Heatmap showing temporal regulation of lipid metabolism gene sets—including steroid metabolism, fatty acid metabolism, and phospholipid metabolism—based on irGSEA scoring across different time points. Gene set enrichment significance was determined by permutation-adjusted p-values (FDR < 0.25 considered significant).

(**C**) Dot plot showing expression of representative genes in cholesterol and fatty acid synthesis pathways stratified by OSBPL3 expression level. Dot size indicates the proportion of expressing cells; dot color reflects average scaled expression.

(**D**) Density plot showing the distribution of steroid biosynthesis gene expression in the high vs. low OSBPL3 expression groups.

(**E**) UMAP dimensionality reduction plots for steroid synthesis, and steroid hormone synthesis pathways.

(**F**) Protein-protein interaction network for OSBPL3 analyzed using the GeneMANIA website.

(**G**) PCA plot showing the spatial distribution of two groups of samples after PLS-DA analysis.

(**H**) Lolipop Plot displaying the top 20 metabolites most strongly correlated with OSBPL3 across different samples.
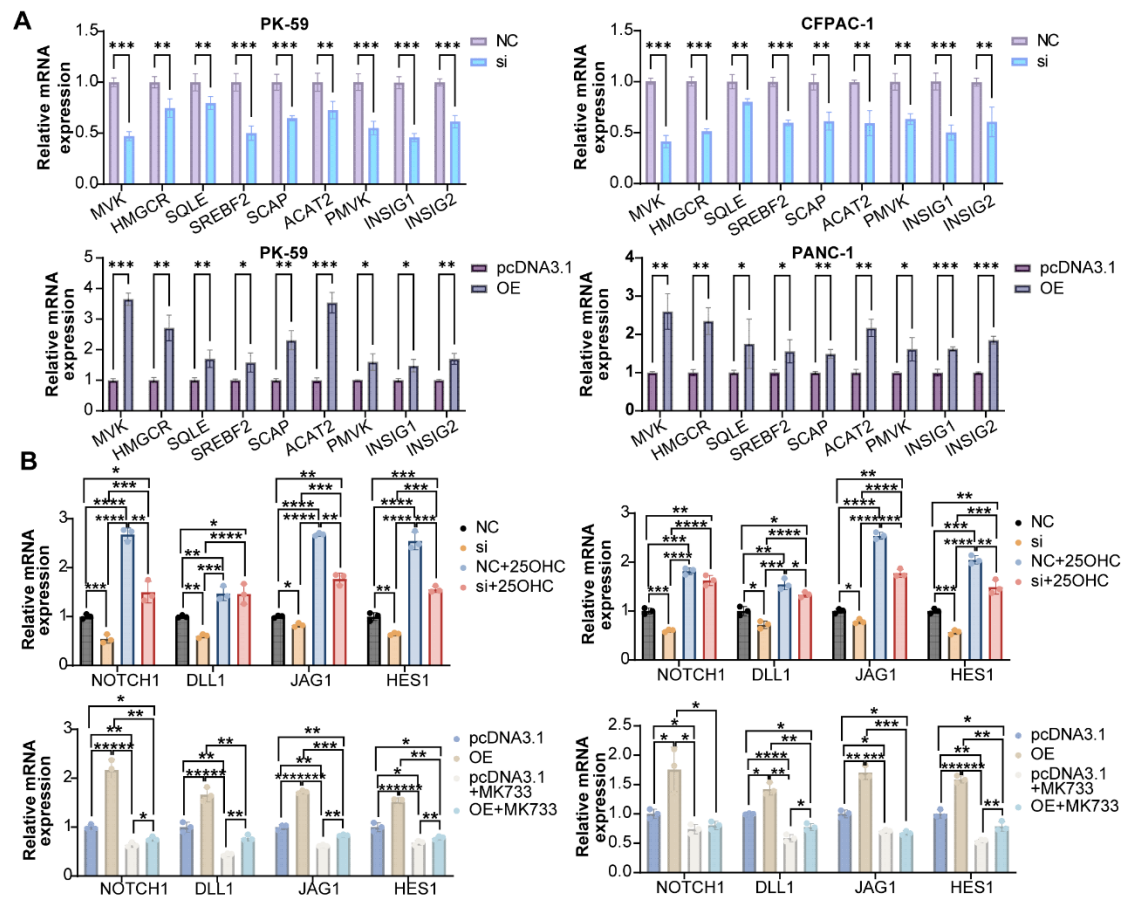
Figure S8. OSBPL3 regulates cholesterol metabolism and NOTCH signaling pathway activity.

(**A**) qRT-PCR analyses were performed to assess the expression levels of key cholesterol related genes in PDA cells before and after OSBPL3 knockdown or overexpression (n = 3).

(**B**) Quantitative real-time PCR (qPCR) analysis of NOTCH pathway related genes NOTCH1, JAG1 and HES1 in OSBPL3-knockdown (CFPAC-1 and PK-59) with 25-hydroxycholesterol (25-OHC, 2.5 µM, 24 h) and OSBPL3-overexpressing (PANC-1 and PK-59) with simvastatin (15 nM, 24 h) treated pancreatic cancer cells. β-actin was used as an internal control.
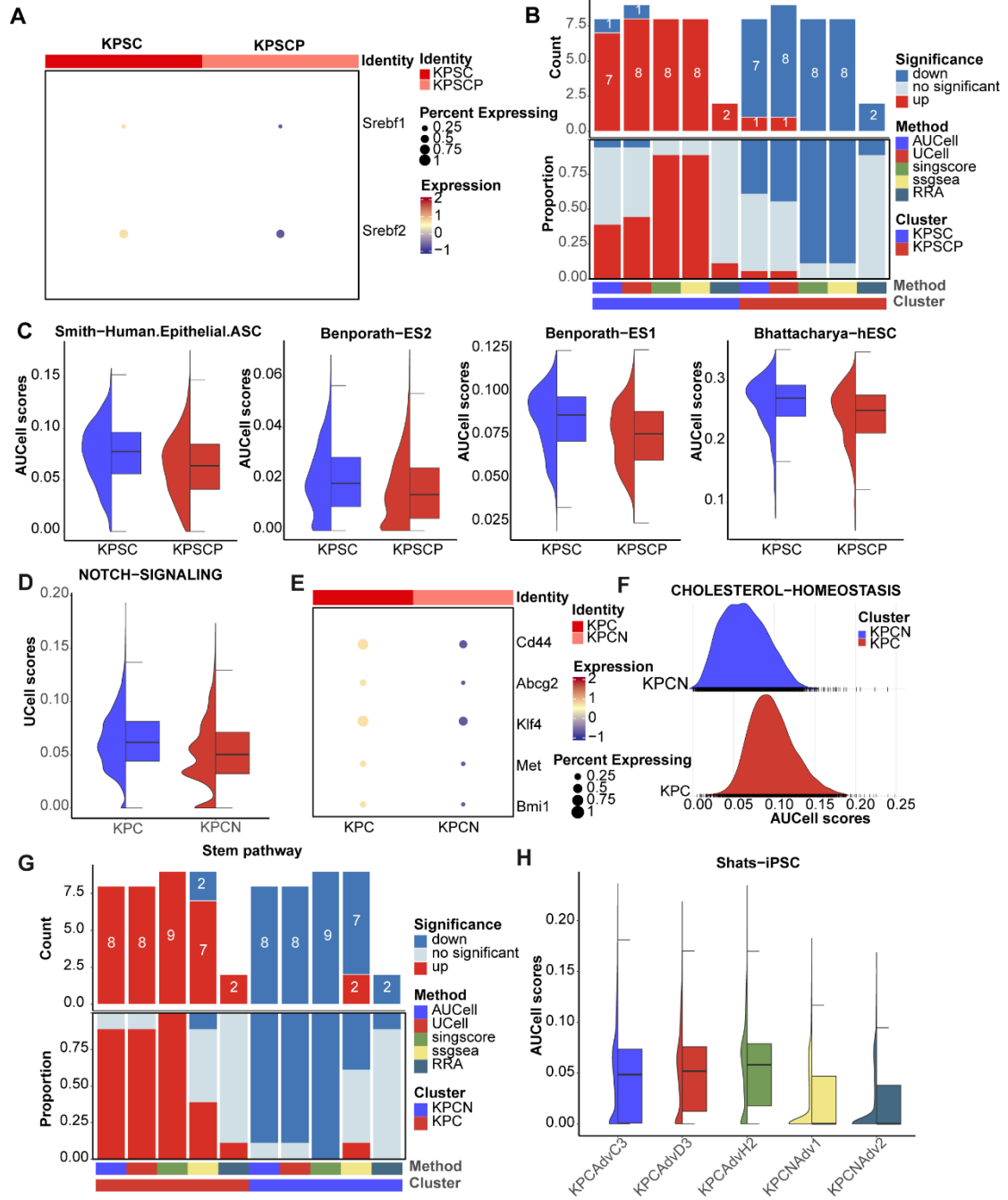
Figure S9. Downregulation of key genes in cholesterol synthesis Inhibits the NOTCH pathway and tumor stemness

(**A**) Bubble plot showing the expression levels of OSBPL3 in KPSC (before) and KPSCP (after) samples from KPC mice following treatment with Perhexiline maleate to inhibit Srebf2.

(**B**) Bar chart displaying the scores for four stemness-related datasets in the KPSC and KPSCP groups, derived from five different algorithms. Red indicates upregulated gene sets, and blue indicates downregulated gene sets.

(**C**) Half violin plot illustrating the AUCell scores for four stemness-related datasets across different samples.

(**D**) Half violin plot showing the UCell scores for the NOTCH pathway in the KPC and KPCN groups before (KPC) and after (KPCN) conditional inactivation of the cholesterol synthesis key enzyme, Nsdhl.

(**E**) Bubble plot presenting the expression levels of stemness-related genes in the KPCN group (KPCNAdv1 and KPCNAdv2) and control KPC group (KPCAdvD3, KPCAdvC3, and KPCAdvH2) samples, following conditional inactivation of Nsdhl.

(**F**) Density plot showing the distribution density of AUCell scores for sterol metabolism-related pathways in KPC and KPCN groups.

(**G**) Bar chart displaying the scores for nine stemness-related datasets in the KPC and KPCN groups, based on five different algorithms. Red represents upregulated gene sets, while blue represents downregulated gene sets.

(**H**) Half violin plot illustrating the AUCell scores for three stemness-related datasets across different samples.